Strip silicon waveguide for code synchronization in all-optical analog-to-digital conversion based on a lumped time-delay compensation scheme*

Sha Li(李莎)[1,†], Zhi-Guo Shi(石志国)[1], Zhe Kang(康哲)[2], Chong-Xiu Yu(余重秀)[2], and Jian-Ping Wang(王建萍)[1]

[1] *School of Computer and Communication Engineering, University of Science and Technology Beijing (USTB), Beijing* 100083, *China*
[2] *State Key Laboratory of Information Photonics and Optical Communications, Beijing University of Posts and Telecommunications (BUPT), Beijing* 100876, *China*

(Received 29 September 2015; revised manuscript received 3 November 2015; published online 20 February 2016)

An all-optical analog-to-digital converter (ADC) based on the nonlinear effect in a silicon waveguide is a promising candidate for overcoming the limitation of electronic devices and is suitable for photonic integration. In this paper, a lumped time-delay compensation scheme with 2-bit quantization resolution is proposed. A strip silicon waveguide is designed and used to compensate for the entire time-delays of the optical pulses after a soliton self-frequency shift (SSFS) module within a wavelength range of 1550 nm–1580 nm. A dispersion coefficient as high as −19800 ps/(km·nm) with ±0.5 ps/(km·nm) variation is predicted for the strip waveguide. The simulation results show that the maximum supportable sampling rate (MSSR) is 50.45 GSa/s with full width at half maximum (FWHM) variation less than 2.52 ps, along with the 2-bit effective-number-of-bit and Gray code output.

Keywords: all-optical analog-to-digital conversion, silicon waveguide, soliton self-frequency shift, time-delay compensation

PACS: 42.65.Tg, 42.65.Re, 42.70.Mp, 42.81.Dp **DOI:** 10.1088/1674-1056/25/4/044210

1. Introduction

An analog-to-digital converter (ADC) is an important part of a communication system which needs to satisfy the requirements for the rapid development of ultra-wide-band applications such as an advanced radar system, high speed optical communication, etc.[1–3] The electrical ADC whose sample rate and art resolution are several giga-samples per second (GSa/s) and 10 bit respectively cannot meet the requirements for ultra-wide-band applications because of its inherent electrical bottle-neck such as clock jitter and sampling aperture, etc.[1–4] The all-optical ADC has attracted much attention because it can overcome the limitation of electronic devices, and meanwhile achieve appropriate quantization resolution and sampling rates. Optical quantization could be realized by soliton self-frequency shift (SSFS), higher-order soliton fission, cross-phase modulation effects, etc.[5–13] Optical quantization utilizing the SSFS effect is a promising option among the above schemes because of its ultrafast response speed, which can realize the sampling rate transparency. The outstanding results in analog-to-digital conversion were given based on the SSFS effect.[14–20] In the process of frequency shift, time-delays between optical pulses with different peak powers occur inherently, leading to the non-synchronization of the quantized optical pulses and coding error. The multiple optical time-delay lines (TDLs) are utilized to compensate for time-delay in the previous schemes whose disadvantages are complicated and expensive. Meanwhile, they cannot meet the demands of miniaturization and photonic integration. Silicon photonic technology is suitable for photonic integration, owing to its compatibility with the complementary metal–oxide–semiconductor (CMOS) process. The optical waves can be confined into the sub-micron region by the high refractive index of silicon by using the silicon-on-insulator (SOI) technology.[21] Some SOI signal processing schemes have been proposed,[22–28] but to the best of our knowledge, there is still no report on an all-optical ADC. The strip waveguide structure on the order of centimeters in length allows for a stronger negative dispersion than conventional fiber and photonic crystal fiber (PCF). However, the organic material requires a non-CMOS process and strict temperature limitation, which renders it unsuitable for mass-manufacturing.[29,30]

In this paper, we propose a lumped time-delay compensation scheme with 2-bit quantization resolution to realize optical pulse synchronization for the first time by inserting a strip silicon waveguide instead of the multiple optical TDLs after the SSFS module. The time-delays between quantized pulses with different peak powers at the output of the silicon wavelength are compensated for. Results based on numerical simulation are discussed.

*Project supported by the Fundamental Research Funds for the Central Universities, China (Grant No. FRF-TP-15-030A1) and China Postdoctoral Science Foundation (Grant No. 2015M580978).

†Corresponding author. E-mail: shalee@ustb.edu.cn

© 2016 Chinese Physical Society and IOP Publishing Ltd

2. Principle of operation

Figure 1 shows an all-optical ADC with 2-bit quantization resolution whose two primary modules are all-optical quantization and coding based on the SSFS effect and optical interconnection, respectively. In Fig. 1, the discrete sampled optical pulses, which can be generated by the four-wave mixing (FWM) effect, are delivered into a span of highly nonlinear fiber (HNLF) to realize a power-to-wavelength conversion based on the SSFS effect. At the output of HNLF, the central wavelength of the spectrum presents a red shift and the shift value is directly proportional to the peak power of the input optical pulse, therefore an arrayed waveguide grating (AWG) is utilized to separate different central wavelengths. Optical signals with different central wavelengths are sent to the specific ports of the AWG and then they are delivered into a coding module. The optical interconnection is realized by using several attenuators, TDLs and photodiodes (PDs) in the coding module. The expressions of outputs b_1 and b_2 are

$$\begin{cases} b_1 = a_1 + a_3, \\ b_2 = a_2 + a_3. \end{cases} \tag{1}$$

By utilizing the optical interconnection, 4 optical pulses (including a pulse with a peak power of 0) are converted into 2-bit Gray codes at outputs of PDs, while the magnitude of the frequency shift corresponds to a Gray code encoding.

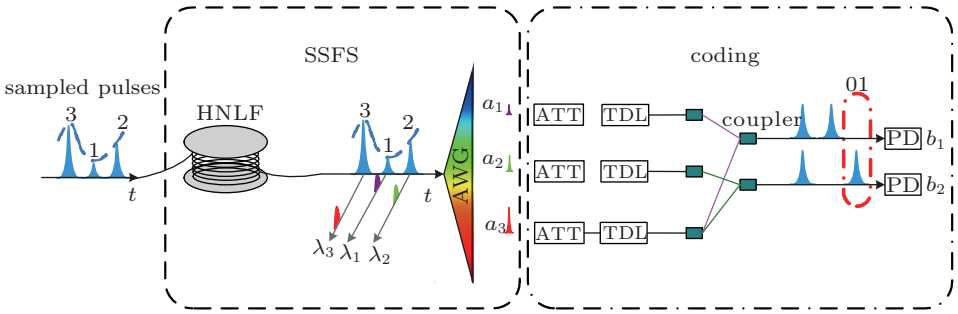


Fig. 1. (color online) Schematic diagram of an all-optical ADC based on SSFS technique. HNLF: highly nonlinear fiber, ATT: attenuator, TDL: time-delay line, PD: photodiode.

All-optical quantization is achieved by the SSFS effect, the central wavelength of the optical pulse presents a red shift. Meanwhile, the optical pulse has a time-delay at the output of the HNLF. The dynamic transmission of sampled optical pulses in HNLF can be described by the simplified generalized nonlinear Schrodinger equation (GNLSE). Solving the GNLSE with the moment method, the time-delay of the sampled pulse Δt can be obtained as follows:[31,32]

$$\Delta t \approx \Delta\Omega \cdot \beta_2 \cdot L \approx \Delta\lambda \cdot D \cdot L = (\lambda_c - \lambda_0) \cdot D \cdot L, \tag{2}$$

where $\Delta\Omega$ is the frequency shift of the sampled pulse, β_2 and L are the second-order dispersion coefficient and the length of fiber, respectively. The dispersion parameter $D = -2\pi c\beta_2/\lambda^2$, λ_c and λ_0 are the central wavelengths of the quantized pulse and initial pulse, respectively. When the dispersion parameter D and the fiber length L are constants, the time-delay Δt is directly proportional to λ_c from Eq. (2). According to the relation between the time-delay and the central wavelength after the SSFS effect, the compensation mechanism is shown in Fig. 2. The blue and red lines represent the time-delay and time-delay compensation curves with slopes of K_1 and K_2, respectively. In order to compensate for the time-delay, the relation $K_2 = -K_1 = (\Delta T_{max} - \Delta T_{min})/(\lambda_{max} - \lambda_{min})$ needs satisfying, while $D_c = K_2/L_c$. Here, D_c and L_c are the dispersion parameter and the length of the lumped time-delay compensation device.

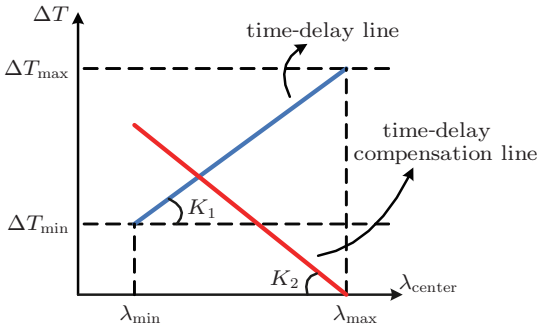


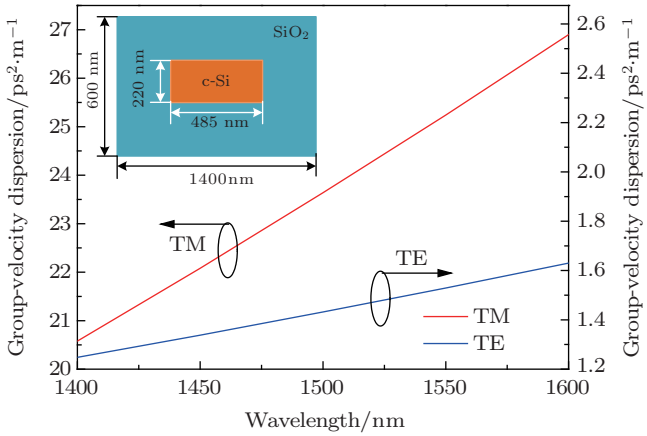
Fig. 2. (color online) Mechanism of the proposed lumped time-delay compensation.

3. Waveguides design and time-delay compensation performance

There are many different ways to realize time-delay compensation as long as the red line can be achieved in Fig. 2, e.g., dispersion compensating fiber (DCF), large dispersion PCF. The group-velocity dispersion (GVD) has a dispersion length $L_D = T_0^2/|\beta_2|$, where T_0 is the initial pulse width and β_2 is the GVD coefficient. The self-phase modulation has nonlinear length $L_{NL} = (\gamma P_0)^{-1}$, where γ is the nonlinear parameter and P_0 is the initial peak power. The dispersion plays a major role, while the nonlinearity is relatively weak, requiring $L \ll L_{NL}$ and $L \approx L_D$, for waveguide length L.

Fortunately, the tight mode confinement in an SOI waveguide helps introduce significant waveguide dispersion

and thus allows one to obtain a dramatically large normal group-velocity dispersion. In other words, a large and flattened negative dispersion parameter is obtained by designing the SOI waveguide appropriately.[33–38] Figure 3 shows the calculated GVD curves for our waveguide. For dimensions of 1400 nm×600 nm and an etching dimension of 485 nm×220 nm (see the inset of Fig. 3). The other parameters of the strip silicon waveguide are shown in the upper right part of Fig. 3. Based on the waveguide structure, the fundamental TM mode exhibits a GVD of 25.24 ps^2/m and a dispersion of −19800 ps/(km·nm) at 1550 nm. Meanwhile, the dispersion variation is ±0.5 ps/(km·nm) from 1400 nm to 1600 nm. This value is 1000 times larger than that of standard silica fiber ($\beta_2 < 0.02$ ps^2/m). With such a high dispersion, the length of the strip silicon waveguide is shorter than that of the conventional fiber or PCF.



Sample	Strip
Coupling loss/dB	6
Propagation loss/(dB/cm)	1.9
Dispersion/(ps/km·nm)	−19800
Im(γ)/W^{-1}·m^{-1}	−5.4
Re(γ)/W^{-1}·m^{-1}	10

Fig. 3. (color online) Calculated dispersion curves for the transverse electric and transverse magnetic modes. The design of our waveguide is shown in the inset, c-Si is the crystalline silicon, and the other parameters of our waveguide are shown in the upper right table.

The lumped time-delay compensation scheme is shown in Fig. 4. Comparing Fig. 4 with Fig. 1, the time-delay compensation is inserted between the quantization module and the coding module. The strip silicon waveguide is brought forward from the HNLF and AWG to realize lumped time-delay compensation rather than multiple TDLs. The improvements are definitely useful for the integration and miniaturization of the all-optical ADC. The dynamic of an optical pulse inside a silicon waveguide is governed by the modified GNLSE, which includes the effects of two-photo absorption (TPA), free-carrier absorption (FCA), and free-carrier dispersion (FCD). The GNLSE is given by

$$\frac{\partial A}{\partial z} = \mathrm{i}\sum_{m=2}^{\infty}\frac{\mathrm{i}^m\beta_m}{m!}\frac{\partial^m A}{\partial t^m} + \mathrm{i}\left(\gamma_0 + \mathrm{i}\gamma_{\mathrm{TPA}}\right)\left(1+\frac{\mathrm{i}}{\omega_0}\frac{\partial}{\partial t}\right)A(z,t) \times \int_{-\infty}^{t} R\left(t-t'\right)\left|A\left(z,t'\right)\right|^2 \mathrm{d}t' - \frac{1}{2}\left(\alpha_l + \alpha_{\mathrm{FCA}}\right)A + \mathrm{i}\frac{\omega_0}{c}n_{\mathrm{FCD}}A, \tag{3}$$

where A is the slowly varying envelope, β_m is the m-th dispersion coefficient, γ_0 and γ_{TPA} are the real and imaginary part of the complex nonlinear coefficient, ω_0 is the center angular frequency of the optical pulse, α_l is the linear loss of the silicon waveguide, α_{FCA} and n_{FCD} are the coefficients of FCA and FCD, which are given by

$$\alpha_{\mathrm{FCA}} = 1.45\times10^{-21}\left(\lambda_0/\lambda_{\mathrm{ref}}\right)^2 N_{\mathrm{c}}$$

and

$$n_{\mathrm{FCD}} = -5.3\times10^{-27}\left(\lambda_0/\lambda_{\mathrm{ref}}\right)^2 N_{\mathrm{c}},$$

with λ_0 and λ_{ref} being the input center wavelength and the reference wavelength, N_{c} being the free-carrier density and given by

$$\frac{\partial N_{\mathrm{c}}}{\partial t} = \frac{\beta_{\mathrm{TPA}}}{2hf_0}\frac{\left|A(z,t)\right|^4}{A_{\mathrm{eff}}^2} - \frac{N_{\mathrm{c}}}{\tau}, \tag{4}$$

where β_{TPA} is the TPA parameter, h is the Plank constant, f_0 is the center frequency, A_{eff} is the effective mode field area of the silicon waveguide, and τ is the effective carrier lifetime.

The nonlinear response function $R(t)$ in Eq. (3) is related to the Raman contribution, and it is defined as $R(t) = (1-f_{\mathrm{R}})\,\delta(t) + f_{\mathrm{R}}h_{\mathrm{R}}(t)$, with f_{R} being the fractional contribution of the nuclei to the total nonlinear polarization. The Raman response function $h_{\mathrm{R}}(t)$ can be deduced from the Raman response spectrum. The Fourier transform $H_{\mathrm{R}}(\Omega)$ of $h_{\mathrm{R}}(t)$ is given by

$$H_{\mathrm{R}}(\Omega) = \frac{\Omega_{\mathrm{R}}^2}{\Omega_{\mathrm{R}}^2 - \Omega^2 - 2\mathrm{i}\Gamma_{\mathrm{R}}\Omega}, \tag{5}$$

where Ω_{R} and Γ_{R} are the Raman shift and the bandwidth of the Raman gain spectrum at room temperature.

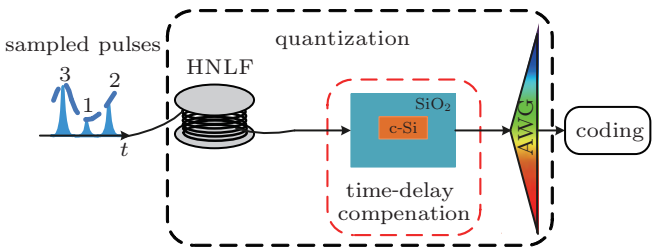


Fig. 4. (color online) Diagram of the lumped time-delay compensation scheme with the silicon waveguide.

4. Simulation and discussion

Solving the GNLSE with the split-step-Fourier method,[31] the dynamic behaviors of the pulses in the time and frequency domain in the quantization process is numerically analyzed. In Fig. 4, a string of hyperbolic secant optical pulses as sampled optical pulses with 0.53 ps full width at half maximum (FWHM), 40-GHz repetition rate and 1550-nm central wavelength is fed into a span of HNLF to present SSFS. To simulate the sampled pulses with different peak powers, a variable optical attenuation (VOA) is used to generate the sampled pulses with different powers. For example, the peak powers Q_1, Q_2, and Q_3 of the sampled pulses are 9.58 W, 12.80 W, and 13.99 W, respectively. Q_0 with a peak power of 0 is of no use in the coding module, so it is neglected in our simulation. After transmitting in a span of HNLF ($\gamma_{\rm HNLF} = 16\ {\rm W}^{-1}{\cdot}{\rm km}^{-1}$, $D_{\rm HNLF} = +3$ ps/(nm·km), $\alpha_{\rm HNLF} = 0.9$ dB/km) for SSFS, the central wavelengths of the sampled pulses are shifted to specific positions. The spectral profiles of the optical pulses Q_1–Q_3 after the HNLF are shown in Fig. 5. The magnitude of the central wavelength shift is in direct proportion to the peak power of the sampled pulse. As shown in Fig. 5, the optical signal is quantized after transmission through the HNLF. It is seen that the spectrum becomes overlapped with each other, which leads to the cross-talk between adjacent channels. Fortunately, the overlap points are all not higher than the FWHM level of the spectrum so that the cross-talk issue can be mitigated with the power equalization by the attenuator array and comparator decision.

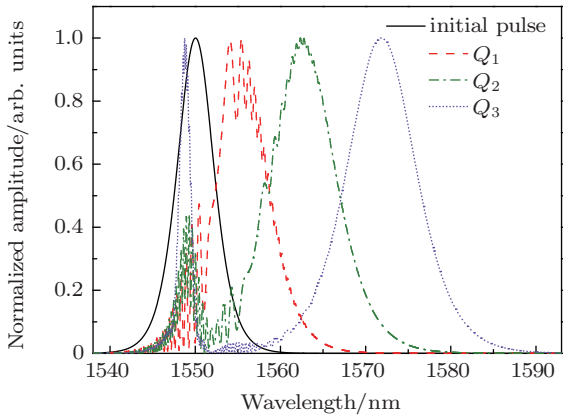


Fig. 5. (color online) Spectral profiles of the optical pulses Q_1, Q_2, and Q_3 after the HNLF.

Figure 6(a) shows the transfer function of the 2-bit AOADC and figure 6(b) shows the differential nonlinear (DNL) and the integral nonlinear (INL) errors calculated from the transfer function, respectively. The transfer function increases monotonically without missing codes. As shown in Fig. 6(a), the least significant bit (LSB) power $P_{\rm LSB}$ and the full-scale of the power range $P_{\rm total}$ are 1.6 W and 6.4 W, respectively. Meanwhile, a peak DNL error of 0.2 LSB and a maximum INL error of 0.2 are obtained.

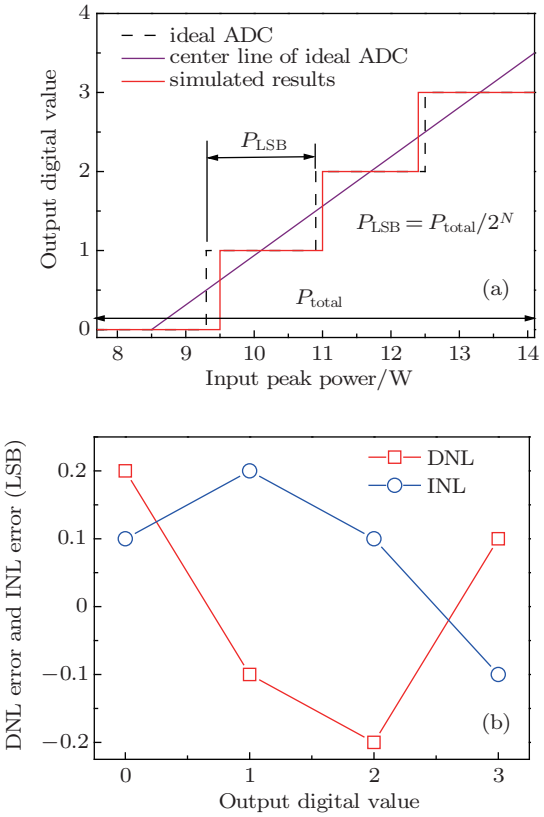


Fig. 6. (color online) (a) Transfer function of the 2-bit AOADC. (b) Differential nonlinear (DNL) error and integral nonlinear (INL) error.

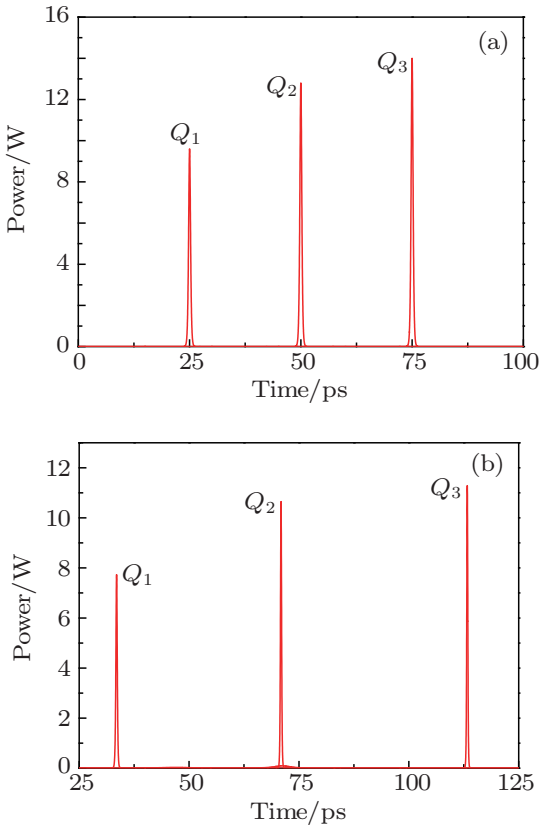


Fig. 7. (color online) (a) Three sampled optical pulses and (b) delayed optical pulses after SSFS.

The initial sampled pulses are recorded in Fig. 7(a). The initial time interval of the adjacent pulses is 25 ps when the

sampling rate is 40 GSa/s. The temporal profiles of the sampled pulses are recorded at the output of the highly nonlinear fiber (HNLF) in Fig. 7(b). After the quantization based on the soliton self-frequency shift (SSFS) effect, the sampled optical pulses with different peak powers have different time-delays. The coding error will be caused by the nonsynchronous issue in the final decision. Adjusting the bandwidth of AWG, the temporal profiles of PD detection and the coding results with time-delay are displayed in Fig. 8(a). Since the input optical pulses are "Q_1, Q_2, and Q_3", the correct codes should be "10 01 11". However, as shown in Fig. 8(a), the coding results are "10 01 00" and the corresponding optical pulses become "Q_1, Q_2, and Q_0", which are inconsistent with the input ones. So the time-delay compensation is quite necessary for ensuring the coding correctness.

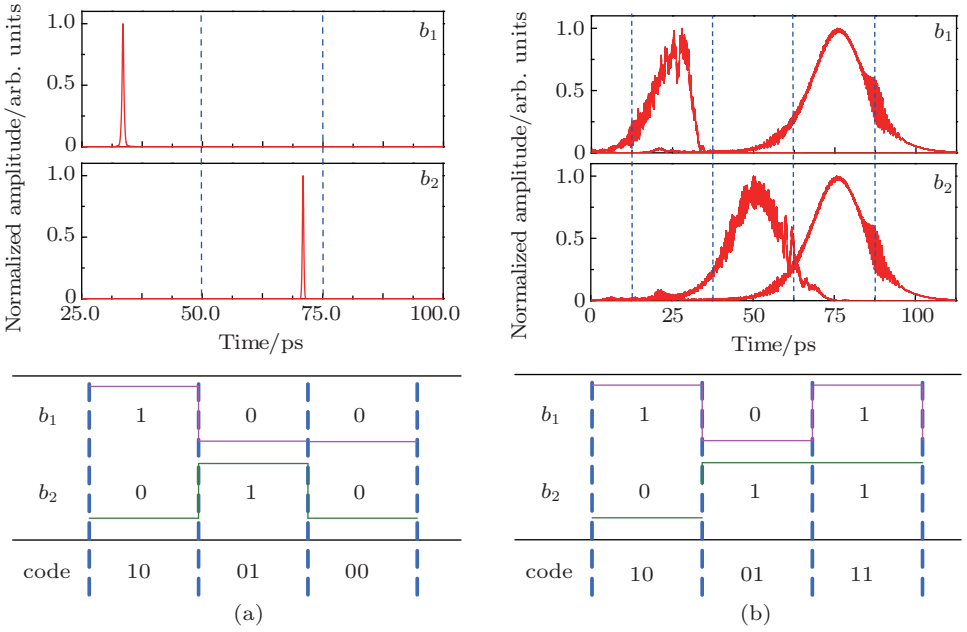


Fig. 8. (color online) Temporal profiles of PD detection and corresponding coding results in two quantization channels for (a) without and (b) with time-delay compensation.

Here, a strip silicon waveguide is utilized to realize lumped time-delay compensation. As shown in Fig. 2, the slope of the time-delay curve is $K_1 = 1.752$ ps/nm in the scheme. Thus, the slope of the time-delay compensation curve is $K_2 = -1.752$ ps/nm. The strip silicon waveguide can be fabricated, starting from SOI wafers patterned with deep-UV lithography, which is a mature technique at present. In Fig. 8(b), the correct binary codes can be obtained based on the lumped time-delay compensation scheme. Because of the large GVD effect, however, the optical pulses after the silicon waveguide are simultaneously broadened. The pulse broadening effect can affect the maximum supportable sampling rate (MSSR) that is defined as

$$\mathrm{MSSR} = \frac{1}{2 \cdot (\text{time-error} + \mathrm{FWHM}_{\text{broadened}}/2)}, \tag{6}$$

where the time-error is the magnitude of the difference between the time position of the compensated pulse and the one of the input pulses, and $\mathrm{FWHM}_{\text{broadened}}$ is the FWHM of the broadened pulses, respectively. From Eq. (6), time-error and $\mathrm{FWHM}_{\text{broadened}}$ are both directly proportional to the reciprocal of the sampling rate. Considering the cases with the GVD fluctuation, the effect of β_2 on the FWHM of the compensated pulses is shown in Fig. 9(a). With the increase of β_2, the FWHM values of the three compensated pulses present fluctuations. However, the variations are relatively slight, which are all less than 2.52 ps. For example, the FWHM of Q_2 is 16.44 ps at the GVD value of 24.44 ps^2/m, and it is 18.96 ps at the GVD value of 25.24 ps^2/m; their difference is only 2.52 ps. In Fig. 9(b), the curve of the time error versus GVD is recorded. The interference of the sampled pulses will occur when the time error is not neglected. With the increase of β_2, Q_1, Q_2, and Q_3 have almost the same time error, and the maximum is 30 ps at the GVD value of 26.24 ps^2/m. Considering both the pulse broadening and GVD fluctuation issues, the curve of MSSR versus GVD is shown in Fig. 9(c) according to Eq. (6). For example, the FWHM of the compensated pulses is 19.82 ps while GVD is 25.24 ps^2/m and the maximum central wavelength is 1572 nm in our scheme, and the sampling rate should be no more than 50.45 GSa/s. With the increase or decrease of GVD relative to 25.24 ps^2/m, the MSSR decreases due to the large dispersion of the strip silicon waveguide.

For the cases where the values of slope K_2 are different, while the dispersion of the silicon waveguide remains constant and the length of the silicon waveguide is changed, the dia-

gram of FWHM, time error and MSSR versus slope K_2 are shown in Figs. 9(d), 9(e), and 9(f), respectively. In our scheme, the FWHMs of the compensated pulses are all slightly fluctuated with the variation of the parameter of the strip silicon waveguide, while the time errors all have relatively large variations correspondingly. The MSSR is mainly determined by the time error in the system based on the strip silicon waveguide. However, the base-order soliton case ($0.5 < N < 1.4$) is met by a VOA before the SSFS module; the effect from the nonlinearity of the silicon waveguide can be neglected.

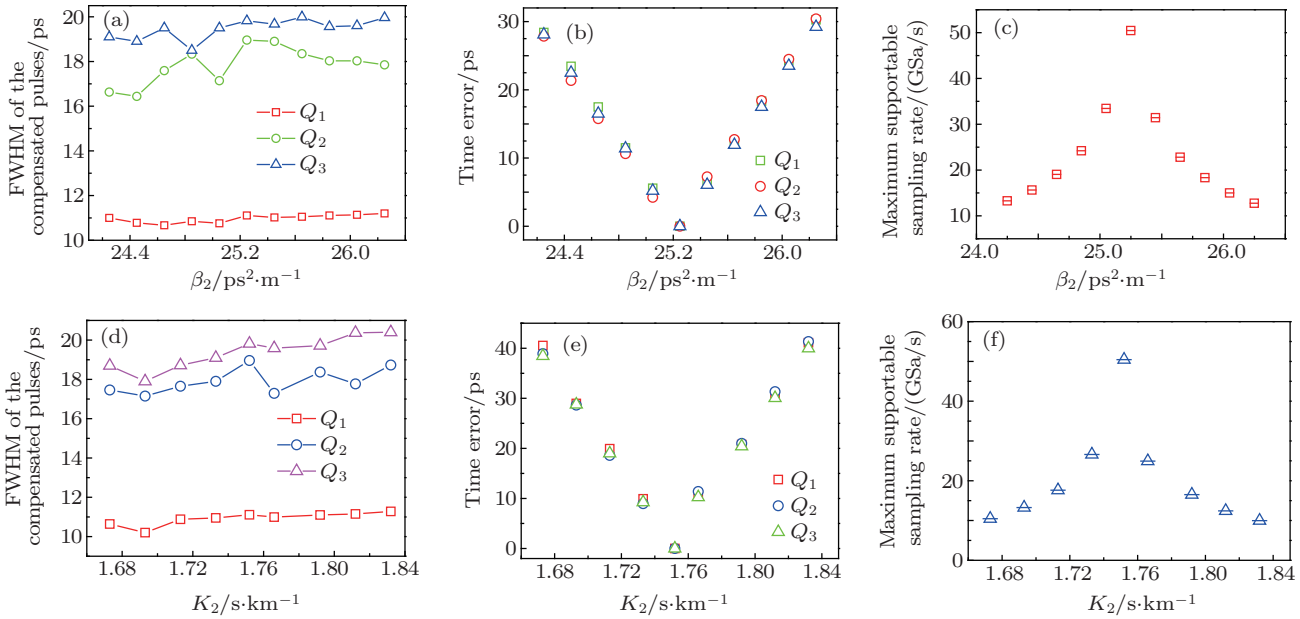


Fig. 9. (color online) (a) Curves of the FWHM versus GVD, (b) the time-error versus GVD and (c) maximum supportable sampling rate (MSSR) versus GVD, (d) the FWHM versus slope K_2, (e) the time-error versus slope K_2, and (f) MSSR versus slope K_2.

The quantization resolution N is defined as

$$N = \log_2\left(\frac{\lambda_{\text{shift}} + \Delta\lambda_{\text{FWHM}}}{\Delta\lambda_{\text{FWHM}}}\right), \tag{7}$$

where λ_{shift} and $\Delta\lambda_{\text{FWHM}}$ are the magnitude of the center wavelength shift and the spectral width of the optical pulse at the output of HNLF. It is obvious that to obtain a large resolution N, a larger λ_{shift} and a smaller $\Delta\lambda_{\text{FWHM}}$ should be achieved. In the present paper, the strip silicon waveguide is utilized to realize time-delay compensation after SSFS instead of DCF or PCF, as well as to meet the demands of miniaturization and photonic integration, which is the development trend of all-optical ADC. Owing to the inherent limitations of length, TPA, FCA, and FCD, it is difficult for the proposed all-optical ADC to realize more than 2-bit quantization. However, it is possible to combine the proposed all-optical ADC with the spectral compression scheme to obtain a smaller $\Delta\lambda_{\text{FWHM}}$ and a higher quantization resolution N after the SSFS module as shown in Fig. 10.

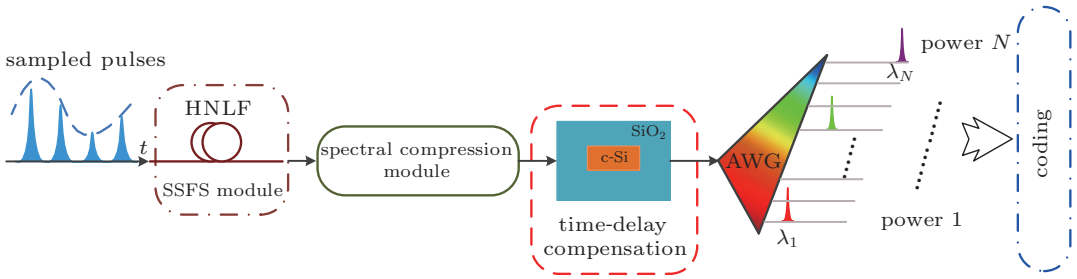


Fig. 10. (color online) Schematic diagram of an all-optical ADC based on the lumped time-delay compensation and the spectral compression modules with more than 2-bit quantization resolution.

5. Conclusions

In this paper, we propose a lumped time-delay compensation scheme based on the silicon waveguide for simplifying the structure and ensuring the coding correctness of the all-optical ADC by SSFS effect. The corresponding TDLs could be replaced by a short silicon waveguide to realize time-delay compensation and integration. The simulation results show that the strip silicon waveguide can compensate for the time-delay accurately with an FWHM variation of less than 2.52 ps. The proposed scheme can support an MSSR of 50.45 GSa/s with

no coding error. When a spectral compression module can be added by utilizing a span of HNLF after the SSFS module, a potential 3-bit resolution can be realized since the total wavelength range is 30 nm. The lumped time-delay compensation scheme utilizing the large dispersion strip silicon waveguide instead of the multiple TDLs and fiber reduces the structure complexity in practical applications, which conforms to the trend of integration and miniaturization of all-optical ADC.

References

[1] Khilo A, Spector S J and Grein M E 2012 *Opt. Express* **20** 4454
[2] Kang Z, Yuan J H and Li S 2013 *Chin. Phy. B* **22** 114211
[3] Xu K, Niu J, Dai Y T, Sun X Q, Dai J, Wu J and Lin J T 2011 *Appl. Opt.* **50** 1995
[4] Valley G C 2007 *Opt. Express* **15** 1955
[5] Ho P P, Wang Q Z, Chen J, Liu Q D and Alfano R R 1997 *Appl. Opt.* **36** 3425
[6] Wei S L, Wu J, Zhao L J, Yao C, Ji C, Lu D, Zhang X L and Yin Z S 2012 *Opt. Lett.* **37** 3699
[7] Tsuyoshi Konishi, Kazunori Tanimura, Kousuke Asano, Yoshinori Oshita and Yoshiki Ichioka 2002 *Opt. Soc. Am. B* **19** 2817
[8] Konishi T, Takahashi K, Matsui H and Satoh T 2012 14th *International Conference on Transparent Optical Networks (ICTON)*, 2012, Coventry, p. 1
[9] Tsuyoshi Konishi, Koji Takahashi, Hideki Matsui, Takema Satoh and Kazuyoshi Itoh 2011 *Opt. Express* **19** 16106
[10] Kang Z, Zhang X T, Yuan J H, Sang X Z, Wu Q, Farrell Gerald and Yu C X 2014 *Opt. Express* **22** 21441
[11] Oda S I, Maruta A and Kitayama K 2004 *Photon. Technol. Lett.* **16** 587
[12] Sho-ichiro Oda, Shu-ichi Okamoto and Akihiro Maruta 2004 *Nonlinear Guided Waves and Their Applications*, Toronto, Canada, p. TuB3
[13] Nishitani T, Konishi T, Furukawa H and Itoh K 2005 *Opt. Express* **13** 10310
[14] Zian Cheak Tiu, Sin Jin Tan, Arman Zarei, Harith Ahmad and Sulaiman Wadi Harun 2014 *Chin. Phys. Lett.* **31** 094206
[15] Wu Z K, Zhang Y Z, Hu Y, Wen F, Zhang Y Q and Zhang Y P 2014 *Chin. Phys. Lett.* **31** 090502
[16] Li Y, Zhu Z Q, Wang X L, Gong L P, Feng S T and Nie S P 2015 *Acta Phys. Sin.* **64** 024204 (in Chinese)
[17] Chen Q C 2014 *Chin. Phys. B* **23** 124212
[18] Takashi Nishitani, Tsuyoshi Konishi and Kazuyoshi Itoh 2007 *Opt. Express* **15** 15812
[19] Nishitani T, Konishi T and Itoh K 2005 *Opt. Rev.* **12** 237
[20] Nishitani T, Konishi T and Itoh K 2008 *IEEE J. Selec. Top. Quantum Electron.* **14** 724
[21] Lin Q, Painter O J and Agrawal G P 2007 *Opt. Express* **15** 16604
[22] Boyraz O and Jalali B 2004 *Opt. Express* **12** 5269
[23] Liu A *et al.* 2007 *Opt. Express* **15** 660
[24] Foster M A, Turner A C, Salem R, Lipson M and Gaeta A L 2007 *Opt. Express* **15** 12949
[25] Almeida V R, Barrios C A, Panepucci R R and Lipson M 2004 *Nature* **431** 1081
[26] Salem Reza, Foster M A, Turner A C, Geraghty D F, Lipson M and Gaeta A L 2008 *Nat. Photon.* **2** 35
[27] Boyraz O 2008 *Nat. Photon.* **2** 12
[28] Sang X Z and Boyraz O 2008 *Opt. Express* **16** 13122
[29] Alejandro Martinez, Javier Blasco, Pablo Sanchis, Jose V Galan, Jaime Garcia-Ruperez and Emmanuel Jordana 2010 *Nano Lett.* **10** 1506
[30] Matres J, Lacava C, Ballesteros G C, Minzioni P, Cristiani I, Fedeli J M, Marti J and Oton C J 2012 *Opt. Express* **20** 23838
[31] Agrawal G P 2007 *Nonlinear Fiber Optics*, 4th edn. (San Diego: Academic)
[32] Liang R 2010 Ph. D. Dissertation, University of Electronic Science and Technology of China, Chengdu, China
[33] Yin L H, Lin Q and Agrawal G P 2006 *Opt. Lett.* **31** 1295
[34] Blanco-Redondo A, Husko C, Eades D, Zhang Y, Li J, Krauss T F and Eggleton B J 2014 *Nat. Commun.* 5, article number 3160
[35] Yin L H and Agrawal G P 2007 *Opt. Lett.* **32** 2031
[36] Zhang J D, Lin Q, Piredda G, Boyd R W, Agrawal G P and Fauchet P M 2007 *Opt. Express* **15** 7682
[37] Shimizu T, Hatori N, Ishizaka M and Yamamoto T 2014 *IEEE CPMT Symposium Japan (ICSJ)*, 2014, Kyoto, p. 55
[38] Yue Y, Zhang L, Yang J Y, Beausoleil R B and Willner A E 2010 *Opt. Lett.* **35** 1364